JGR – Oceans: 2016JC012070

Title: Remote sources for year-to-year changes in the seasonality of the Florida Current transport

Ricardo Domingues[1,2,*] Molly Baringer[2], and Gustavo Goni[2]

[1] Cooperative Institute for Marine and Atmospheric Studies, University of Miami, Miami, FL, USA

[2] Atlantic Oceanographic and Meteorological Laboratory, NOAA, Miami, FL, USA

*corresponding author

Ricardo.Domingues@noaa.gov

4301 Rickenbacker Causeway, Miami, FL 33149, USA

Running Title: Remote sources of seasonal FC changes

Key Points

1. The seasonal variability of the Florida Current (FC) transport exhibits year-to-year changes during the 1983-2013 record.
2. Year-to-year changes in the FC seasonality are linked with westward propagating signals (WPS) originated in the eastern North Atlantic.
3. Coastal sea-level changes forced by WPS account for ~50% of the FC seasonal variability that is linked with variable annual phase.

Draft version 7, August 12, 2016

Abstract

The seasonal variability of the Florida Current (FC) transport is often characterized by the presence of an average annual cycle (8% of the variance) of ~3 Sv range peaking in boreal summer. However, the seasonality displayed by the FC transport in any individual year may have very distinct characteristics. In this study, the analysis focuses on seasonal changes (73—525 day frequency band) in the FC transport that are associated with a variable annual phase, which is defined as the transient seasonal component (FCt, 27% of the variance). It is shown that the FCt is largely modulated by westward propagating sea height anomaly (SHA) signals that are formed in the eastern North Atlantic 4 to 7 years earlier than observed at 27°N in the Florida Straits. These westward propagating SHA signals behave approximately like first baroclinic Rossby waves that can modulate changes in the FC seasonal variability upon arrival at the western boundary. The main finding from this study is that changes in coastal sea-level between 25°N—42°N linked with westward propagating signals account for at least 50% of the FCt. The integrated changes in the coastal sea-level between 25°N—42°N, in turn, drive adjustments in the geostrophic transport of the FC at 27°N. Results reported here provide an explanation for previously reported year-to-year changes in the FC seasonality, and suggest that large sea-level variations along the coast of Florida may be partially predictable, given that these Rossby-wave-like signals propagate approximately at fixed rates in the open ocean along 27°N.

Keywords: Baroclinic Rossby waves, Mesoscale Eddies, Western Boundary Currents, Satellite altimetry, Florida Current cable

1. Introduction

The Florida Current (FC) is the western boundary current closing the subtropical gyre circulation in the North Atlantic Ocean that carries both the return flow associated with the wind-driven gyre, and the upper branch of the Meridional Overturning Circulation (MOC). The FC flow has been described in numerous studies as having an annual cycle in transport with range of ~3 Sv (1 Sv = 10^6 m^3 s^{-1}) and maximum transport in July [e.g. Niiler and Richardson, 1973; Baringer and Larsen 2001; Beal et al., 2008; Meinen et al., 2010]. The leading theory is that the FC annual cycle is predominantly forced by the along-channel wind stress in the Florida Straits and by wind stress curl [e.g. Schott et al., 1988; DiNezio et al., 2009; Rousset and Beal, 2011]. Modern observations and modeling experiments have revealed the importance of additional processes that can influence the FC seasonal variability, such as the local eddy field [Frajka-Williams et al., 2013], and baroclinic signals coming from the ocean interior [Ezer, 1999; Sturges and Hong, 2001; Czeschel et al., 2012].

Changes in the strength of the FC have been observed and described within different frequency bands [Baringer and Larsen 2001; Meinen et al., 2010], with particular focus on the changes in its transport that occur with annual periodicity. Year-to-year changes in the FC annual cycle were first reported by Baringer and Larsen [2001], who identified substantial differences in the annual transport between 1982—1990 and 1991—1998. During 1982—1990 the FC had an amplified (~5 Sv) annual cycle, peaking in July, while during 1991—1998 the FC had lower range (~1.5 Sv) annual variations and a pronounced semi-annual cycle. In addition, during 2000—2007, the FC also showed a weak semi-annual cycle [Meinen et al., 2010]. Atkinson et al. [2010] confirmed the marginally statistically significant changes in the FC annual cycle, and speculated that transport variability at non-seasonal time scales could cause changes in the annual variability of this current. These studies focused on seasonal averages computed over long periods of time using a continuous record of the FC volume transport, which provides an average overview of seasonal changes in the FC transport that occur at fixed annual phases. This focus on fixed annual phase emphasizes deterministic forcing essentially driven by the annual cycle of solar forcing (and hence implied wind forcing) and de-emphasizes dynamical internal forcing mechanisms. In this paper we define signals with seasonal variability but variable annual phase – *transient seasonal variability* – that allow us to more fully examine the stochastic and dynamic forcing. Herein, the "transient seasonal component of the FC transport" (FCt) is defined as variability within the 73—525 day frequency band that is associated with variable annual phase (average annual cycle removed).

One potential source of seasonal variability for the FC transport is semi-annual/annual first baroclinic Rossby waves observed in the North Atlantic [Polito and Liu, 2003; Clément et al., 2014]. In fact, modeling studies suggest that baroclinic signals coming from the ocean interior may drive a relevant component of the FC seasonal variability [Czeschel et al., 2012]. Analysis of *in situ* and satellite altimetry observations suggest that 42% of the MOC variance inferred from geostrophic calculations in the ocean interior at 26.5N can be attributed to first mode variability linked with eddies and Rossby waves at periods of 8-250 days [Clément et al., 2014]. In the FC, while observational evidence suggests that first baroclinic Rossby waves are linked with changes in the FC transport at the 3—12 years frequency band [DiNezio et al., 2009], an analysis focused on the semi-annual/annual band may provide additional insight on the seasonal variability induced by remotely forced signals. Because the signals of first baroclinic Rossby waves and of westward propagating mesoscale eddies are often superimposed in the sea surface height anomaly (SHA) data [Oliveira et al., 2013; Polito and Sato, 2015], the generic term westward propagating signals is adopted here for convenience.

The goal of this study is to show that signals originating in the eastern North Atlantic can largely explain the transient seasonal variability of the FC transport. It will be also shown that the variability linked with the westward propagating signals provides a mechanism for explaining the previously reported changes in the seasonal variability of the FC transport [Baringer and Larsen, 2001;

Atkinson et al., 2010; Meinen et al., 2010]. Understanding such changes in the FC seasonality is important given that the FC is an important component of the climate system that carries the upper-branch of the MOC, especially because seasonal changes in the Meridional Heat Transport (MHT) and MOC are closely linked with the FC and western boundary circulation [Boning and Rudich, 1991; Elipot et al., 2014]. In addition, changes in the strength of the FC are largely associated with coastal sea-level variability [Blaha, 1984; Ezer, 2016] and sea-level rise along the east coast of U.S. [Ezer, 2013; Ezer et al., 2013], which is of ultimate importance for the resilience of coastal communities and ecosystems. Therefore, because changes in the FC transport can be linked to physical processes that may lead to societal impacts, efforts aiming to improve the understanding of mechanisms driving such changes in the FC are important.

This manuscript is organized as follows: in section 2, the FC transport time-series is introduced and analyzed; in section 3, the characteristics of the westward propagating signals in the North Atlantic are described; in section 4, the impact of westward propagating signals on the seasonality of the FC transport is quantified; in section 5, year-to-year changes in the FC seasonality are examined and the anomalous westward propagating signals responsible for inter-annual variations in FC annual cycles are discussed; and in section 6, the main findings of this work are summarized.

2. Variability of the FC transport

Since 1982, NOAA has provided daily FC transport measurements using a submerged abandoned telephone cable crossing the Florida Straits at 27°N, 79°W—80°W [Larsen, 1992; Baringer and Larsen, 2001; Meinen et al., 2010] as part of the Western Boundary Time Series project. These data are made available at the NOAA/Atlantic Oceanographic and Meteorological Laboratory website (www.aoml.noaa.gov/phod/floridacurrent/). Daily FC transport data are used to investigate the potential links between changes in the FC transport and the westward propagating signals.

Time-series of FC transport (Figure 1a) during 1983—2013 has an average volume transport of ~32 Sv, with root mean square (RMS) of 3.4 Sv. The average annual cycle peaks in boreal summer, and has a peak-to-peak range of 2.8 Sv (Figure 1a). The wavelet transform of the FC transport (Figure 1b) indicates that the FC has variability in different frequency bands, and that there were significant changes in the spectral characteristics of the current throughout the record. Variability significant at the 95% confidence interval is observed for: (a) the high-frequency band with periods less than 73 days; (b) an intermediate frequency band with semi-annual and annual periods within the 73—525 days range enclosed by the magenta lines; and (c) the low-frequency band with two-year periodicity. Changes in the low-frequency spectral characteristic of the FC transport may be linked with the reported interannual adjustments in the wind stress curl related with the North Atlantic Oscillation (NAO) [Baringer 2001; Atkinson et al., 2010]. In this study, focus is given to the band at periods of 73-525, which is defined following the inspection of the wavelet transform diagram of the FC transport (Figure 1b): the lower and upper limits of 0.2 year (73 days) and 1.44 year (~525 days), respectively, are defined to ensure that the dominant annual and semi-annual signals are included in the transient FC component, which is used here to assess year-to-year changes seasonality of the transport linked with westward propagating signals. Analysis reveals that the total variability of the FC transport during 1983—2013 is partitioned into: (i) 53% due to high-frequency variability (<73 days, RMS = 2.4 Sv); (ii) 35% due to changes in transport within the 73—525 day frequency band (RMS = 1.9 Sv); and (iii) 12% due to low-frequency variability (> 525 days, RMS = 1.1 Sv). The 73-525 day cutoff is defined to exclude high-frequency and low-frequency signals that are not likely relevant for processes studied here, while still permitting a good representation of semi-annual and annual signals. The variability within the 73—525 day frequency band may be further decomposed: 8% due to the average annual cycle (RMS = 0.8 Sv, Figure 1a); and 27% due to seasonal variability linked with variable annual phase that is defined here as the transient seasonal component (FCt, RMS = 1.7 Sv, Figure 1a). The FCt has an absolute range of ~8 Sv and its contribution to the total variability is threefold when compared to the average annual cycle exhibited by the FC transport, causing the observed year-to-year changes in the seasonality of this current (Figure 1c). Thus, the FCt corresponds to a large portion of the total FC variability. Extreme values of FCt smaller (larger) than the 5% (95%) percentile were observed on April 1986, February 1994, and June 1996 (July 2000, September 2004, and December 2008) (Figure 1a). Ocean conditions during these events are further analyzed below.

3. Westward propagating signal in the North Atlantic

The links between the semi-annual/annual westward propagating signals in the North Atlantic and the FC variability are evaluated using SHA data from satellite altimetry, obtained from the AVISO. In order to examine processes likely to impact the seasonality of the FC, the time scales associated with these signals must be included. In the following analysis, the equivalent transient seasonal component of the SHA time-series (SHAt) is computed by filtering the data for the 73—525 day frequency band after removing the average annual cycle computed over the period from 1993—2013. This frequency band includes the dominant westward propagating signals with semi-annual and annual period in the North Atlantic [Polito and Liu, 2003], and accounts for ~42% of the total SHA variability along 27°N west of 60°W. The field of mean Eddy Kinetic Energy (EKE) derived from SHAt data during 1993—2013 is the largest in the subtropical North Atlantic between 35 – 42°N and west of 35°W due to the Gulf Stream variability (Figure 2). The Azores Current can be identified from the elevated EKE values extending from 32 – 36°N, 50 – 20°W. Elevated EKE is also clearly evident in the Loop Current region (22 – 28°N, 95 – 85°W) and near the Antilles Current and recirculation of the subtropical gyre (22 – 28°N, 76 – 65°W).

Longitude-time Hovmoller diagrams of SHAt in the North Atlantic are analyzed here for: (a) 27°N, (b) 34°N, and (c) 40°N (Figure 3a,b,c), based on the regions of largest EKE variability described above. These diagrams show slanted patterns indicative of westward propagating signals. The average westward propagating phase speeds estimated by following individual phases are -4.6 ± 1.4 km day^{-1}, -2.4 ± 0.8 km day^{-1}, and -1.7 ± 0.3 km day^{-1}, for 27°N, 34°N, and 40°N, respectively. These phase speeds imply that signals originating in the eastern North Atlantic (5°W—15°W) take approximately four, six, and seven years to reach the east coast of the United States (U.S.) at 27°N, 34°N, and 40°N, respectively. The phase speeds calculated here are within one standard deviation of previous estimates in the North Atlantic [Polito and Liu, 2003; Watanabe et al., 2016]. At all latitudes evaluated here, the estimated speeds are approximately 40—60% faster than the speeds predicted by standard linear theory for long first baroclinic Rossby waves estimated using the World Ocean Atlas 2013 [Locarnini et al., 2013; Zweng et al., 2013]: -2.9 ± 0.7 km.day^{-1} at 27°N, -1.7 ± 0.3 km.day^{-1} at 30°N, and -1.0 ± 0.3 km.day^{-1} at 40°N. Faster than linear westward phase speeds are commonly observed in the real ocean because values of β and of the internal radius of deformation (Rd) calculated from standard linear theory neglect other important components setting the actual background potential vorticity gradient [the effective-β, Watanabe et al., 2016], such as large-scale baroclinic flow in the oceans [Killworth et al., 1997].

Spectral analysis of the SHAt data as a function of longitude (Figure 3d,e,f) reveals (i) the westward amplification of the westward propagating signals, (ii) the presence of seasonal variability, and (iii) the rapid attenuation of the signals approaching the western boundary (continental slope). The westward amplification of the spectral power associated with westward propagating signals is often associated with interaction with the bottom topography [Chelton and Schlax, 1996], and / or the background circulation [Cipollini et al., 1997]. The westward amplification of the signal is also evident in the longitude-time diagrams (Figure 3a,b,c). For example, at 27°N the SHAt on the eastern side of the basin ranges between -3 cm and +3 cm, while at the western side the SHAt ranges between -20 cm and +20 cm (Figure 3a). The amplification of the westward propagating signals illustrates the intensification of the circulation towards the west. The striking persistence of significant seasonal periodicity implies the presence of transient seasonal variability; in other words, the westward propagating signals are associated with seasonal periodicity with variable annual phase. These results suggest that these signals conserve their spectral (wavelength and period) characteristics while crossing the North Atlantic Ocean, which may partly because dissipation due to diapycnal eddy diffusivity is small in the ocean interior ($\sim 0.1 \times 10^{-4}$ m^2 s^{-1}), whereas enhanced dissipation is usually observed near sloping topography, where values often exceed $1 \times 10^{-4} m^2 s^{-1}$ [Toole et al., 1994]. The implications of the transient seasonal variability for the FC variability will be discussed in section 4. The rapid decay in the spectral power close to the western boundary is consistent with the mechanism proposed by previous studies [Kanzow et al., 2012]: it results from the fact that velocities perpendicular to the coast are physically unrealistic, implying that along boundary pressure gradients/anomalies must dissipate quickly.

Westward propagating signals discussed in this study are largely linked with wind-driven mechanisms. Previous studies have shown that these signals may be generated by local wind forcing in the ocean interior due to Ekman Pumping [Krauss and Wuebber, 1982], and also by wind stress variations on the eastern boundary that can lead into changes in the depth of the thermocline [Anderson and Gill, 1975; Krauss and Wuebber, 1982]. The detailed analysis reported by Watanabe et al., (2016) based on the comparison of a minimalistic wind forced Rossby wave model with satellite winds and altimetry observations showed that the main forcing mechanism is due to wind stress variations on the eastern boundary of the basin. This is likely the main reason why the variability of signals observed here can be traced to the eastern boundary.

Observations indicate that coherent SHAt are observed along the east coast of the U.S. between 26.5°N—42°N (not shown here); for example SHAt along the coast are correlated with the sea level at 27°N with lags of less than 1 week. These observations are generally consistent with previous studies

[Mooers et al, 2005; Ezer, 2013; Ezer et al., 2013; Ezer 2016], and imply that changes in the coastal sea-level at 27°N are associated with the variability associated with westward propagating signals that is rapidly transmitted along the coast. In a study using idealized model simulations, Huthnance [2004] showed that large-scale ocean motions could be indeed transmitted to the shelf through the generation of coastally trapped waves, which in the North Atlantic Ocean, imply in southward phase propagation along the east coast of U.S. In fact, Ellipot et al. [2013] found pressure signals traveling south as fast as ~128 m s^{-1} along the east coast of the U.S., which was hypothesized to represent the propagation of near-barotropic coastally trapped waves. The rapid transmissions of signals along the coast will rapidly force changes in the sea-level in the Florida Straits, which will then contribute to changes in the FC transport.

4. Remote sources of FC variability

Changes in the FC transport at frequencies lower than the local inertial period are directly associated with changes in the cross-stream sea-level gradient; this is due to the geostrophic balance between the cross-stream pressure gradient force and the Coriolis force (along-stream velocity). Therefore, negative anomalies in the FC transport are linked with sea-level rise on the western edge of the current (Florida), and with sea-level fall on its eastern edge (Bahamas). Lagged correlation coefficients between the FCt and the SHAt are evaluated across the Atlantic basin to investigate potential links between the variability of the FC transport and westward propagating signals. At zero lag (Figure 4a), the spatial distribution of the correlation coefficients is consistent with the geostrophic balance discussed above, with positive correlation coefficients on the eastern edge of the FC, and negative correlation coefficients on the western edge. In this analysis, negative correlation coefficients at zero lag are of interest, because changes in sea-level along the coast of Florida are negatively correlated with the FC transport; this is a decrease in sea-level at the Florida coast that coincides with an increase in the FC transport. The lagged correlation analysis reveals correlation coefficients observed for zero lag between the FCt and the SHAt at the Florida Straits that can be consistently traced across the North Atlantic along 27ºN (Figure 4b). Even though non-linear effects become more evident at 34ºN and 40ºN (Figure 4c,d), similar correlation patterns are also observed in these latitudes. The slanted pattern observed in the lagged correlation analysis indicates a potential first order linear connection between the FCt variability with the SHAt variability in the eastern side of the basin, even though non-linear processes play an important role in the dynamics of westward propagating signals in subtropical latitudes [Watanabe et al., 2016]. Because phase speeds for individual wave crests can vary with longitude in subtropical regions [Polito and Liu, 2003], out-of-phase waves can interfere with the linear correlation between FCt and SHAt signals in the eastern North Atlantic. Still, correlation lags imply that signals formed ~4.5 years earlier on the eastern boundary may modulate the seasonality of the FC transport once they reach the western boundary. Similarly, at 34°N (40°N), negative correlations between the FCt and SHAt at the western boundary can also be traced to the eastern North Atlantic, implying lags of ~6.4 (~7.3) years. The negative correlation coefficients obtained for analysis along the east coast of the U.S. indicate that positive SHAt formed on the eastern North Atlantic are linked with a reduction in the FC flow once these signals reach the western boundary years later.

In fact, a closer analysis of the SHAt data (Figure 5) indicates that during extreme FCt events (Figure 1), the spatial SHAt distribution is consistent with the slow down or intensification of the transport, and that such SHAt signals can be indeed traced to the ocean interior. For example, negative SHAt values observed on the Bahamas edge of the FC and positive SHAt values along the U.S. coast on February 11 1994 (Figure 5a) were consistent with the small value of FCt observed for this date (Figure 1). Further analysis of the SHAt data two months (Figure 5b) and four months (Figure 5c) before this event confirms that the negative SHAt signal originated in the ocean interior. A similar SHAt distribution showing negative values on the Bahamas edge of the FC on June 21 1996 (Figure

5d) also coincided with small values of FCt. During the occasions when the FCt exhibited an extreme large value, the SHAt distribution was characterized by an approximately opposite pattern, with positive SHAt values on the Bahamas edge of the FC, and negative SHAt values along the U.S. coast (Figure 5g,j). These observations are consistent with results from previous studies [Frajka-Williams et al., 2013], which reported that anticyclonic eddies (positive SHA) originating east of the Bahamas may cause an increase in the Antilles Current and in the FC transports on seasonal time scales. These relationships found between SHAt signals and FCt are indicative of geostrophic adjustments in the transport of this current.

Results described above imply that the seasonal variability of the FC transport may be partly modulated by signals formed 4—7 years earlier in the eastern North Atlantic. This delayed response of the FC to westward propagating signals corresponds to changes in the strength of the western boundary current due to baroclinic adjustments in the subtropical gyre. Anderson and Corry [1985] recognized that baroclinic signals formed in the eastern North Atlantic may take years to decades to reach the western boundary. In addition, they also concluded that baroclinic adjustments in the gyre forced by seasonal changes in large-scale winds were unlikely to explain the seasonal variability of the FC. Our analysis shows that seasonal SHA signals formed in the eastern North Atlantic may conserve their spectral characteristics while traveling across the basin, and can modulate the FC seasonal variability upon arrival at the western boundary, which corresponds to a relevant component of the total variance.

The correlation coefficients between the FCt and SHAt for different latitudes (Figure 4b,c,d) also indicate that changes in FC transport are not just associated with westward propagating signals reaching the western boundary at 27°N, but that different latitude bands can combine, resulting in a net change in the FC transport. Along the U.S. coast, coherent changes in SHA were negatively correlated with the FC transport. These results suggest that coastally trapped waves may provide the main link between the open ocean variability associated with westward propagating signals and the modulation of the FC transport. For example, results from Ezer (2016) based on idealized numerical simulations showed that imposed changes in the FC flow could lead to coherent variations in the Gulf Stream transport along its the entire path, which often caused the generation of coastally trapped signals that could feedback into the FC variability. The interaction between westward propagating signals and the Gulf Stream may drive a similar effect, leading to the generation coastally trapped waves that can modulate the FC seasonal variability. To evaluate this mechanism, SHAt time-series are obtained at 80 locations along the east coast of the U.S. (Figure 6a) to quantify the percentage of the FCt variance that can be accounted for by SHAt along the coast. First, in order to evaluate the applicability of satellite altimetry data at the coast for the transient seasonal band, time-series of SHAt are compared to *in situ* sea-level data from 10 tide gauges along the east coast of U.S., which were obtained from the University of Hawaii Sea-Level Center. Time-series of sea-level data from tide gauges shown here are: (1) de-tided; (2) corrected for the inverse barometer effect using fields of atmospheric pressure at the surface from NCEP's North America Regional Reanalysis; and (3) filtered for the transient seasonal band. Comparisons between coastal SHAt and filtered sea-level data from the tide gauges (Table 1) exhibit correlation coefficients larger than 0.7 (significant at the 99% confidence level), which indicates that altimetry derived SHAt time-series can be good proxies of coastal sea-level variability for this region for the frequency-band evaluated in this study (73—525 days). It should also be noted that sea-level variability along the western boundary may be caused by other processes in addition to westward propagating signals. Most of these processes, however, are either explicitly removed by altimetry corrections [see AVISO, 2013], or implicitly removed by using the cutoff frequencies employed in this study [see Ezer et al., 2013].

In order to quantify the percentage of the FC transport that can be explained by coastal SHAt, the following steps are applied: (1) the time-series of SHAt from the 80 locations along the coast are decomposed into principal components (PCs) and empirical orthogonal functions (EOFs); (2) the main

PCs accounting for 95% of the combined SHAt variability are selected; (3) the selected PCs are used as predictors for FCt in a multivariate linear regression method (Equation 1); and (4) the explained variance (R^2) is quantified. The application of step (1) provides two main advantages: (a) it reduces the number of time-series used by the multivariate linear regression method from 80 to a maximum of 10 time-series, which reduces errors due to artificial covariance in the underlying time series; and (b) it ensures that the multivariate linear regression is not based on an ill-posed linear system, since PCs are constructed to be independent from each other. Step (3) consists of solving:

$$\begin{bmatrix} A_1 \\ \vdots \\ A_m \end{bmatrix} = \left(X^T \times X\right)^{-1} \times X^T \times Y \tag{1}$$

where A is a vector matrix containing the slope coefficients, and

$$X = \begin{bmatrix} PC_{1,t=1} & \cdots & PC_{m,t=1} \\ \vdots & \ddots & \vdots \\ PC_{1,t=n} & \cdots & PC_{m,t=n} \end{bmatrix}, \text{ and } Y = \begin{bmatrix} FCt_{t=1} \\ \vdots \\ FCt_{t=n} \end{bmatrix}$$

The subscripts *m* and *n* indicate the number of PC time-series used, and the length of the time-series, respectively, while the superscripts X^T and X^{-1} denotes the transpose and inverse of matrix X. To further evaluate the contribution of signals within specific latitude bands to the FC variability, steps (1) through (4) are repeated 80 times by progressively including the coastal SHAt time-series from south to north. Physically, this approach enables the evaluation of the relationship between the FC transport and integrated sea-level changes along the coast, since fast barotropic signals can propagate as fast as 128 m s^{-1} (~10,600 km day^{-1}) along the east coast of U.S. [Elipot et al., 2013].

Results from this approach reveal that while only ~20% of the FCt variance can be explained by SHAt time-series at the Florida Straits (25°N, Figure 6b), the use of combined SHAt time-series between 25°—42°N may represent up to ~50% of the FCt variance; the explained FCt variance increases with the introduction of additional SHAt time-series from south to north in the multivariate linear regression. In a few latitude bands (e.g. 25°N—29°N, 35°N—36°N, and 39°N—42°N, Figure 6b), the percentage of explained FCt variance increases rapidly. On the other hand, in other latitude bands (e.g. 30°N—35°N, and 36°N—39°N), a relatively steady value is estimated. Latitude bands with an abrupt increase in the explained variance coincide with the location of important geographical features along the east coast of U.S., such as (a) the northern edge of the Bahamas archipelago at 27.5°N; (b) Cape Hatteras at 35.5°N; and (c) Cape Cod at 41.6°N. Specific components of sea-level variability at the east coast of the U.S. may be confined to narrow latitude bands due to: (1) blocking effects exerted by the Bahamas archipelago on westward propagating waves; (2) baroclinic waves induced or modified by the Gulf Stream [e.g., Ezer, 2013]; and (3) sharp changes in coastline orientation at Cape Hatteras and Cape Cod that may affect the coastal waveguide. For example, the bottom topography can play an important role on accelerating sea-level rise around Cape Hatteras [Ezer, 2013], and also on blocking the southward propagation of baroclinic coastal waves [Ezer, 2016]. The inherent physics of western boundary regions imply that all these components must be transmitted southward along the stream towards the Florida Straits. However, the existence of independent SHA components downstream from the Florida Straits indicates that some of these components may be partially masked/modified by coastal effects (e.g. due to bottom topography), and may not be represented on time-series from the Florida Straits. These results indicate that westward propagating signals reaching the FC / Gulf Stream in different locations along the U.S. coast may account for approximately 50% of the FC transient seasonal variability. These results are complementary to the findings of Clément et al. [2014], who reported that 42% of the MOC variance inferred from geostrophic calculations in the ocean interior at 26.5ºN can be attributed to first mode variability linked with these westward propagating signals.

To further investigate the links between coastal sea-level seasonal variability and changes in the

FCt, slope (Figure 6c), coefficients from the linear regression between the FCt and coastal SHAt are analyzed. In most locations along the east U.S. coast (blue bars, Figure 6c), a decrease of 5—7cm in sea-level is coincident with an increase of 1 Sv in the FCt. On the eastern side of the Florida Straits adjacent to the Bahamas (red bar shown in Figure 6c), an increase of 5cm in sea-level is linked with a 1 Sv increase in FCt. Similar results from this analysis are also obtained using filtered sea-level time-series derived from tide gauges data (triangles, Figure 6c). Hence, observed FCt transport values ranging between -4 Sv and 4 Sv imply sea-level changes along most of the east U.S. coast and the Bahamas of between -20 cm and 20 cm.

Coastal sea-level changes and rise along the U.S. coast have been previously associated with adjustments in the geostrophic dynamics of the FC and Gulf Stream [Ezer, 2013; Ezer et. al., 2013]. To further verify that the observed sea-level changes reported here were also linked with adjustments in the geostrophic dynamics of the FC, values reported here are compared with values expected from simple geostrophic calculations. For example, taking into account that the Coriolis parameter has a value of $6.6 \times 10^{-5}\ s^{-1}$ at 27ºN, that the area of the Florida Straits is ~$4.5 \times 10^{7}\ m^{2}$, and assuming a barotropic adjustment in the water column, a 5 cm change in coastal sea-level across the Florida Straits would result in a ~3 Sv change in the FC transport, which is three times larger than values observed here (~5cm / 1 Sv, Figure 6c). Assuming a baroclinic adjustment instead, where the Florida Straits area is replaced by the area of the water column above the thermocline (~$1.8 \times 10^{7}\ m^{2}$), the calculation results in a transport anomaly of 1.2 Sv, which is very close from values observed here. Therefore, these results indicate that coastal sea-level changes reported in this study for the U.S. coast may be largely linked with fluctuations in the FC transport above the thermocline, suggesting baroclinic adjustment in the geostrophic circulation.

5. Year-to-year changes in the FC seasonality

Changes in the seasonality of the FC transport and the coastal SHAt variability caused by westward propagating signals will certainly produce inter-annual changes in the annual cycle (Figure 7a). For example, the historical record of the FC indicates that high values of transport are generally found during July-September (black line, Figure 1c). While the FC transport exhibits high values during July-September in 1983—1985, 1987—1989, 2004, 2009, and 2013, low values are observed during these months in 1991—1992, 1996—1999, 2006—2008, and 2011 (Figure 7a). These year-to-year changes in the seasonal variability of the FC transport are consistent with results reported by previous studies [Baringer and Larsen, 2001; Meinen et al., 2010], which noted changes in the FC annual cycle during 1982—1990 from those recorded during 1991—1998, and 2000—2007. Figure 7b shows that the predicted FCt_{SHA} largely captures the changes in the seasonality in the observed FCt (Figure 7a). For example, seasonal changes in the FCt during 1995—1997 and 2004—2005 (Figure 7a) were well described by FCt_{SHA} (Figure 7b). This result further supports the hypothesis that the transient seasonal variability of the FC transport is a direct consequence of the integrated sea-level changes along the western boundary and with westward propagating signals reaching the coast (see section 3). In addition, the extreme values of FCt (Figure 1a and Figure 7a) are largely reproduced in FCt_{SHA} (Figure 7b), providing further evidence that such extreme changes in the FC seasonality can be predicted by using westward propagating signals (Figure 5) in the eastern Atlantic. On some occasions, however, the seasonal variability exhibited by FCt is only partially reproduced by FCt_{SHA}, such as during 2010—2013 (Figure 7a,b). Differences between FCt and FCt_{SHA} indicate the existence of other mechanisms for driving seasonal changes in the FC transport, such as those caused by year-to-year changes in the wind forcing [Meinen et al., 2010; Dinezio et al., 2009], and/or by changes in conditions upstream from the Florida Straits, for example at the Loop Current [Rousset and Beal, 2011]. For example, extreme values of the NAO observed during 2009-2010 were linked with changes in the wind field and attributed as the one of the main drivers for the extreme low value of the North Atlantic MOC observed during this period at 26.5ºN [McCarthy et al., 2012; Ezer, 2015; Srokosz and Bryden, 2015]. Therefore, it is likely that similar interannual NAO-related changes in the wind field may lead to adjustments in the transient seasonal component of FC transport that can overlap or even outweigh the effect of westward propagating signals at times. Finally, the average annual cycle and the transient component of the FC seasonal variability are linked with seasonal changes in the transport with range of ~3 Sv and ~8 Sv, respectively. This implies that constructive interactions between these two components may lead to an amplified annual cycle within a given year. Likewise, canceling effects between the average annual cycle and the transient components may occasionally lead to a weak or non-existent annual cycle of the FC. Constructive interactions between these two components may potentially explain the amplified annual cycle observed during 1982—1990 (outside the satellite altimetry period), which had an amplitude of approximately 5 Sv [Baringer and Larsen, 2001; Meinen et al., 2010].

6. Conclusions

In this study, the time-series of FC transport derived from telephone cable voltage measurements in the Florida Straits is analyzed along with sea-level data from tide gauges and from satellite altimetry to investigate a mechanism linking seasonal changes in the FC transport with signals formed in the eastern North Atlantic 4—7 years earlier. The analysis focused on the period during 1993—2013 when high quality satellite altimetry data is available. To investigate year-to-year changes in the seasonality of the FC transport, the concept of transient seasonal variability of the FC transport (FCt) was defined as the variability within the 73—525 day frequency band associated with variable annual phase (average annual cycle removed). The FCt component accounts for 27% of the total FC variability, and shows values ranging between -4 Sv and 4 Sv around the mean FC transport of ~32 Sv.

The main finding from this study is that year-to-year changes in the FC seasonality (represented as FCt) are largely (at least 50%) modulated by westward propagating signals originating in the eastern North Atlantic 4—7 years earlier. These westward propagating signals travel through the North Atlantic conserving their spectral characteristics, leading to changes in the FC transport upon their arrival at the western boundary. The rationale behind this mechanism is that westward propagating perturbations in the free-surface cause changes in the cross-stream pressure gradient at the FC and adjustments in the geostrophic transport once the perturbations reach the western boundary. Westward propagating signals, or perturbations in the free-surface, were identified using altimetry-derived SHA data filtered from the transient seasonal band (SHAt), which corresponds to the dominant component of SHA variability (42% of total variance) in the proximity of the western boundary region in the North Atlantic. An analysis using coastal SHAt time-series between 25°N—42°N showed that integrated changes in sea-level in the U.S. coast and Bahamas account for up to 50% of the FCt variability, indicating that seasonal adjustments in the FC transport can occur when westward propagating signals reach the western boundary. Physically, the evaluation of integrated sea-level changes along the coast provides a robust way of accounting for components of the sea-level variability at the coast that may be partially masked at their individual locations by coastal effects (e.g. due to bottom topography). The importance of these findings lies in the fact that seasonal changes in FC transport correspond to an important component of the MOC and MHT seasonal variability.

Another important finding from this study is to report the existence of key locations along the U.S. east coast where changes in sea-level included relevant 'predictors' of the FCt seasonal variability. These key locations coincide with important features along the east coast of the U.S., namely: (a) the northward edge of the Bahamas archipelago at 27.5°N; (b) the location of Cape Hatteras at 35.5°N; and (c) the location of Cape Cod at 41.6°N. We conclude that specific components of sea-level variability, such as those coming from the Gulf Stream, may be confined to narrow latitude bands possibly due to sharp changes in coastline orientation at Cape Hatteras and Cape Cod. More importantly, the areas where little additional information is added to help better predict the FCt means that in these three distinct regions the variability is consistent, meaning there are three distinct dynamical regimes along the east coast (between 25° and 42°N).

It is also shown that the average annual cycle and the transient seasonal component of the FC seasonal cycle are linked to transport changes with ranges of 3 Sv and 8 Sv, respectively, which potentially explains the previously reported year-to-year changes in the FC annual cycle [Baringer and Larsen, 2001; Meinen et al., 2010]. Constructive (destructive) interactions between these two components may potentially explain the amplification (weakening) of the FC annual cycle previously reported for 1982—1990 (1991—1998) by Baringer and Larsen [2001].

In conclusion, the results obtained in this study from a joint analysis of *in situ* and satellite-derived data emphasize the critical importance of analysis combining different datasets that can provide key information about the dynamics and variability of ocean currents. Our results also provide additional understanding of the relationship of mesoscale signals and of the wind-driven gyre to the western boundary current's variability. Further modeling-based studies are currently being carried out to assess the specific mechanisms by which westward propagating signals interact with the FC. This work also highlights the importance of the global ocean observing system, and in particular, the value of combining data from satellite observations with sustained in situ observations.

Acknowledgments

The Florida Current cable and section data are made freely available on the Atlantic Oceanographic and Meteorological Laboratory web page (www.aoml.noaa.gov/phod/floridacurrent/). The altimetry products were produced by Ssalto/Duacs, distributed by AVISO, and supported by the CNES (available at http://www.aviso.oceanobs.com). Science quality sea-level data from tide gauges along the east coast of the U.S. is produced and distributed by the University of Hawaii Sea—Level Center (available at: http://uhslc.soest.hawaii.edu/). North America Regional Reanalysis—NARR—data were provided by the NOAA/OAR/ESRL PSD, Boulder, Colorado, USA, (available at: http://www.esrl.noaa.gov/psd/). The authors would like to thank Dr. Shenfu Dong, Dr. Elizabeth Johns, and two anonymous reviewers for helpful comments on the manuscript. This research was partly carried out under the auspices of the Cooperative Institute for Marine and Atmospheric Studies (CIMAS), University of Miami, and funded by the Climate Observations Division of the NOAA Climate Program Office and by the NOAA Atlantic Oceanographic and Meteorological Laboratory.

References

Anderson, D. L. T., and R. A. Corry (1985), Ocean response to low frequency wind forcing with application to the seasonal variation in the Florida Straits—Gulf Stream transport. *Prog. Oceanogr.*, *14*, 7-40.

Anderson, D. L., and Gill, A. E. (1975). Spin-up of a stratified ocean, with applications to upwelling. In Deep-Sea Res., 22(9) , 583-596.

Atkinson, C. P., H. L. Bryden, J. Hirschi, and T. Kanzow (2010), On the seasonal cycles and variability of Florida Straits, Ekman and Sverdrup transports at 26 N in the Atlantic Ocean. *Ocean Sci.*, 6(4), 837-859.

AVISO (2013), User Handbook Ssalto/Duacs: M(SLA) and M(ADT) Near-Real Time and Delayed-Time, SALP-MU-P-EA-21065-CLS, edition 3.6, September 2013.

Baringer, M. O. N., and J. C. Larsen (2001), Sixteen years of Florida Current transport at 27 N. *Geophys. Res. Lett.*, *28*(16), 3179-3182.

Beal, L. M., J. M. Hummon, E. Frajka-Williams, O. B. Brown, W. Baringer, and E. J. Kearns (2008), Five years of Florida Current structure and transport from the Royal Caribbean Cruise Ship Explorer of the Seas. *J. Geophys. Res.: Oceans (1978–2012)*, *113*(C6).

Blaha J. P., (1984), Fluctuations of monthly sea level as related to the intensity of the Gulf Stream from Key West to Norfolk. J. Geophys. Res.: Oceans, 89(C5), 8033-8042.

Boning, C. W., and R. G. Budich (1991), Seasonal transport variation in the western subtropical north-atlantic: Eperiments with an eddy-resolving model, *J. Phys. Oceanogr.*, 21, 1271–1289.

Chelton, D. B., and Schlax, M. G. (1996). Global observations of oceanic Rossby waves. Science, 272(5259), 234.

Clément, L., Frajka-Williams, E., Szuts, Z. B., and Cunningham, S. A. (2014), The vertical structure of eddies and Rossby waves and their e act on the Atlantic MOC at 26 N, J. Geophys. Res., 119, 6479–6498, doi:10.1002/2014JC010146, 2014. 2713, 272

Cipollini, P., Cromwell, D., Jones, M. S., Quartly, G. D., and Challenor, P. G. (1997), Concurrent altimeter and infrared observations of Rossby wave propagation near 34 N in the Northeast Atlantic. *Geophys. Res. Let.*, 24(8), 889-892.

Czeschel, L., C. Eden, and R. J. Greatbatch (2012), On the driving mechanism of the annual cycle of the Florida Current transport. *J. Phys. Oceanogr.*, 42(5), 824-839.

DiNezio, P. N., L. J. Gramer, W. E. Johns, C. S. Meinen, and M. O. Baringer (2009), Observed year-to-year variability of the Florida Current: Wind forcing and the North Atlantic Oscillation. *J. Phys. Oceanogr.*, 39(3), 721-736.

Elipot, S., C. Hughes, S. Olhede, and J. Toole (2013), Coherence of western boundary pressure at the RAPID WAVE array: boundary wave adjustments or deep western boundary current advection? *J. Phys. Oceanogr.*, 43(4), 744-765.

Elipot, S., E. Frajka-Williams, C. Hughes, and J. Willis (2014), The observed North Atlantic MOC, its meridional coherence and ocean bottom pressure, *J. Phys. Oceanogr.*, 44, 517–537, doi:10.1175/JPO-D-13-026.1, 2722

Ezer, T., (1999), Decadal variabilities of the upper layers of the subtropical North Atlantic: an ocean model study. J. Phys. Oceanogr., 29(12), 3111-3124. doi:10.1175/1520-0485(1999)029

Ezer, T. (2013), Sea level rise, spatially uneven and temporally unsteady: Why the US East Coast, the global tide gauge record, and the global altimeter data show different trends. *Geophys. Res. Lett., 40*(20), 5439-5444

Ezer, T., L. P. Atkinson, W. B. Corlett, and J. L. Blanco (2013), Gulf Stream's induced sea level rise and variability along the US mid-Atlantic coast. *J. Geophys. Res.: Oceans*., *118*(2), 685-697.

Ezer, T. (2015), Detecting changes in the transport of the Gulf Stream and the Atlantic overturning circulation from coastal sea level data: The extreme decline in 2009-2010 and estimated variations for 1935-2012, Global Planet. Change, 129, 23-36, doi:10.1016/j.gloplacha.2015.03.002.

Ezer, T., (2016), Can the Gulf Stream induce coherent short-term fluctuations in sea level along the U.S. East Coast?: A modeling study, Ocean Dynam., 66(2), 207-220, doi:10.1007/s10236-016-0928-0.

Frajka-Williams, E., W. E. Johns, C. S. Meinen, L. M. Beal, and S. A. Cunningham (2013), Eddy impacts on the Florida Current. *Geophys. Res. Lett*., *40*(2), 349-353.

Huthnance, J. M., (2004), Ocean-to-shelf signal transmission: a parameter study. J. Geophys. Res., 109(C12029). doi:10.1029/2004JC002358.

Killworth, P. D., D. B. Chelton, and R. A. de Szoeke (1997), The speed of observed and theoretical long extratropical planetary waves. *J. Phys. Oceanogr.*, 27(9), 1946-1966.

Krauss, W., and Wuebber, C. (1982). Response of the North Atlantic to annual wind variations along the eastern coast. Deep-Sea Res., 29(7), 851-868.

Larsen, J. (1992), Transport and heat flux of the Florida current at 27 degrees N derived from cross-stream voltages and profiling data: Theory and observations, Philosophical Transactions of the Royal Society of London. Series A: Physical and Engineering Sciences, 338(1650), 169–236.

Locarnini, R. A., and Coauthors (2013), World Ocean Atlas 2013. Vol. 1: Temperature. A. Mishonov, Technical Ed. NOAA Atlas NESDIS, 73, 40pp.

McCarthy, G., Frejka-Williams, E., Johns, W.E., Baringer, M.O., Meinen, C.S., Bryden, H.L., Rayner, D., Duchez, A., Roberts, C., Cunningham, S.A., (2012). Observed interannual variability of the Atlantic meridional overturning circulation at 26.5°N. Geophys. Res. Lett. http://dx.doi.org/10.1029/2012GL052933.

Meinen, C. S., M. O. Baringer, and R. F. Garcia (2010), Florida Current transport variability: An analysis of annual and longer-period signals. *Deep Sea Res., Part I*, *57*(7), 835-846.

Mooers C.N.K., C.S. Meinen, M.O. Baringer, I. Bang, R. Rhodes, C. N. Barron, and F. Bub. (2005), Cross Validating Ocean Prediction and Monitoring Systems. EOS, 86(29):269,272-273.

Niiler, P. P., and W. S. Richardson (1973), Seasonal variability of the Florida Current. *J. Mar. Res*, *31*(3), 144-167.

Oliveira, F. S., and P. S. Polito (2013), Characterization of westward propagating signals in the South Atlantic from altimeter and radiometer records. *Remote Sens. Environ.*, 134, 367-376.

Polito, P. S., W. T. Liu (2003), Global characterization of Rossby waves at several spectral bands. *J. Geophys. Res.: Oceans*., (1978–2012), 108(C1).

Polito, P. S., and O. T. Sato (2015), Do eddies ride on Rossby waves?. *J. Geophys Res.: Oceans*, 120(8), 5417-5435.

Rousset, C., and L. M. Beal (2011), On the seasonal variability of the currents in the Straits of Florida and Yucatan Channel. *J. Geophys. Res.: Oceans*., *116*(C8), C08004.

Schott, F. A., T. N. Lee, and R. Zantopp (1988), Variability of structure and transport of the Florida Current in the period range of days to seasonal. *J. Phys. Oceanogr.*, *18*(9), 1209-1230.

Srokosz, M. A., and H. L. Bryden (2015), Observing the Atlantic Meridional Overturning Circulation yields a decade of inevitable surprises. Science, 348(6241). doi:10.1126/science.1255575.

Sturges, W. B., Hong, G., [2001], Gulf Stream transport variability at periods of decades. J. Phys.

Oceanogr. 31, 1304-1312.

Toole, J. M., K. L. Polzin, R. W. Schmitt (1994), Estimates of diapycnal mixing in the abyssal ocean, Science, 264, 1120-1123.

Watanabe, W. B., P. S. Polito, and I. C. da Silveira (2016), Can a minimalist model of wind forced baroclinic Rossby waves produce reasonable results? *Ocean Dynam.*, pp.1-10.

Zweng, M. M., and Coauthors (2013), World Ocean Atlas 2013, Vol. 2: Salinity. S. Levitus, Ed., A. Mishonov Technical *Ed. NOAA Atlas NESDIS* 74, 39 pp.

Figure Captions & Tables

Table 1 – Correlation coefficients between SHAt at the coast derived from satellite altimetry and *in situ* sea-level data from tide gauges. The time-frame used on the regression analysis is shown below.

Location	Time-frame	Location	Correlation
Bahamas	1993-2003	078° 59.0’W / 26° 41.4’N	0.76
Virginia Key, FL	1996-2012	080° 09.7’W / 25° 43.9’N	0.89
Port Canaveral, FL	1994-2012	080° 35.6’W / 28° 24.9’N	0.89
St. Augustine, FL	1993-2003	081° 15.7’W / 29° 51.4’N	0.85
Mayport, FL	1993-2001	081° 25.9’W / 30° 23.7’N	0.85
Ft. Pulaski, GA	1993-2012	080° 54.1’W / 32° 02.0’N	0.76
Charleston, SC	1993-2012	079° 55.5’W / 32° 46.9’N	0.82
Wilmington, NC	1993-2012	077° 57.2’W / 34° 13.6’N	0.65
Lewes, DE	1993-2011	075° 07.2’W / 38° 46.9’N	0.65
Nantucket, MA	1993-2012	070° 05.8’W / 41° 17.1’N	0.72

Figure 1. (a) Florida Current transport time-series (thin gray line) derived from voltage differences across the Florida straits using telephone cables. Highlighted are the average annual cycle (thick red line) during 1983—2013 and the transient seasonal component (FCt, thick blue line), which is the focus of this study. Arrows indicate extreme events when the FCt was smaller than the 5% percentile (cyan arrows) or larger than the 95% percentile (orange arrows). (b) Wavelet spectrum density for the FC transport time-series (gaps in the time-series were filled with white noise). The thick white contours represent the peak-based significance levels, computed at 95%. The thick black curve indicates the cone of influence. (c) Seasonality displayed by the FC transport during 1983—2013. The annual cycle (thick black line) in panel (c) was calculated as daily averages from the daily FC cable dataset from 1983—2013, and then smoothed using a 30-day running mean filter.

Figure 2. Altimetry-derived Eddy Kinetic Energy for the 73—525 days frequency band.

Figure 3. Longitude-time Hovmoller diagram of filtered SHA along the following latitudes: (a) 27°N, (b) 34°N, and (c) 40°N. Normalized spectrum of the SHA for each longitude averaged between: (c) 27°N, (d) 34°N, and (e) 40°N. The green arrow in (d) indicates the location of the Florida Straits. Note that the same SHA scale was used for each and hence peak values of ± 20 cm at 27°N are obscured (see text).

Figure 4. (a) Geographic distribution of correlation coefficients at zero lag between SHAt and the FCt at each grid point. The marker "+" indicate locations where correlation coefficients are not significant at the 95% confidence level. Lagged correlation coefficients plotted as a function of longitude (abscissa) and of correlation lag (ordinate) between the FCt and the SHAt along: (b) 27°N, (c) 34°N, and (d) 40°N. The green lines and arrow in panels (a) and (b) emphasize the location of the Florida

Straits at 27°N.

Figure 5. Maps of SHA data filtered for the transient seasonal band for the dates displayed. Arrows on the upper right corner on panels (a), (d), (g), and (j) indicates dates of extreme events when the FCt was larger than the 95% percentile (orange arrows) or smaller than the 5% percentile (cyan arrows). Specific positive (negative) westward propagating signals are emphasized by the green (yellow) shaded contours.

Figure 6. (a) Location of altimetry-derived SHAt time-series used in this work (colored circles) and of the tide gauges (green triangles) used to validate the coastal SHAt. The color of the circles indicates the correlation coefficient of individual SHAt time-series with the FCt. (b) Percentage of the explained FC variance as function of latitude (thick black line) and 95% confidence level (black dashed line). The right axis indicates the number of significant PCs time-series (gray bars) derived from the coastal SHAt that were used in the multivariate linear regression. (c) Absolute values of linear regression slope coefficients in cm/Sv between coastal SHAt time-series and the FCt (colored bars). Similar slope coefficients derived using filtered tide gauges data are also shown (triangles). Negative slope coefficients from locations along the east U.S. coast are shown in blue, while positive slope coefficients from the Bahamas are shown in red.

Figure 7. (a) FCt plotted as a function of years (ordinate) and months (abscissa) in order to emphasize changes in the annual phase of the FC transport. (b) Same as (a) but for the FCt_{SHA}. Squares indicate extreme events emphasized in the text for periods when the FCt was larger than the 95% percentile (orange squares), or smaller than the 5% percentile.

Figure 1. Figure

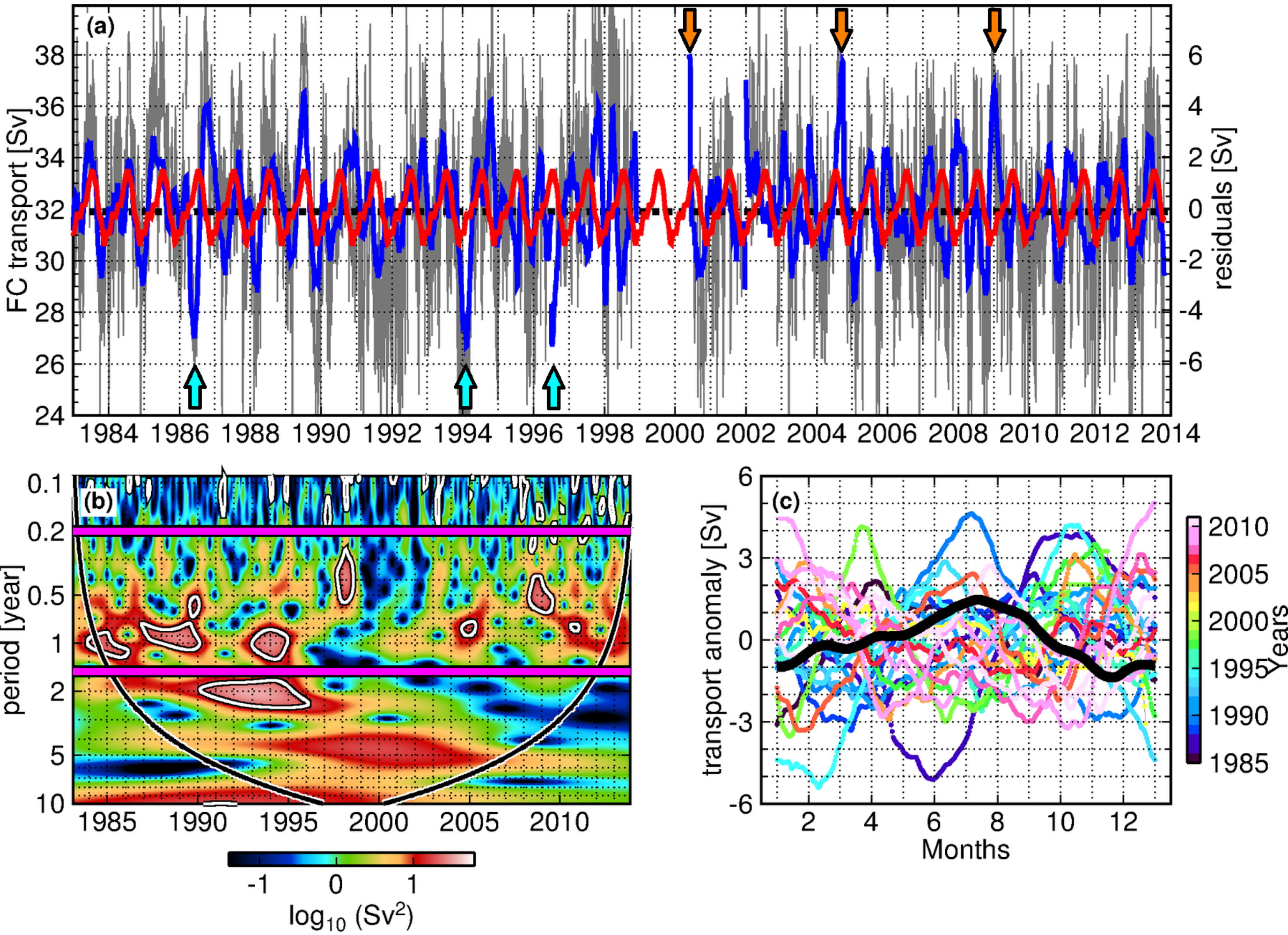

(a)
FC transport [Sv]
residuals [Sv]
24 26 28 30 32 34 36 38
-6 -4 -2 0 2 4 6
1984 1986 1988 1990 1992 1994 1996 1998 2000 2002 2004 2006 2008 2010 2012 2014
(b)
period [year]
0.1 0.2 0.5 1 2 5 10
1985 1990 1995 2000 2005 2010
-1 0 1
log10 (Sv2)
(c)
transport anomaly [Sv]
-6 -3 0 3 6
2 4 6 8 10 12
Months
Years
1985 1990 1995 2000 2005 2010

Figure 2. Figure

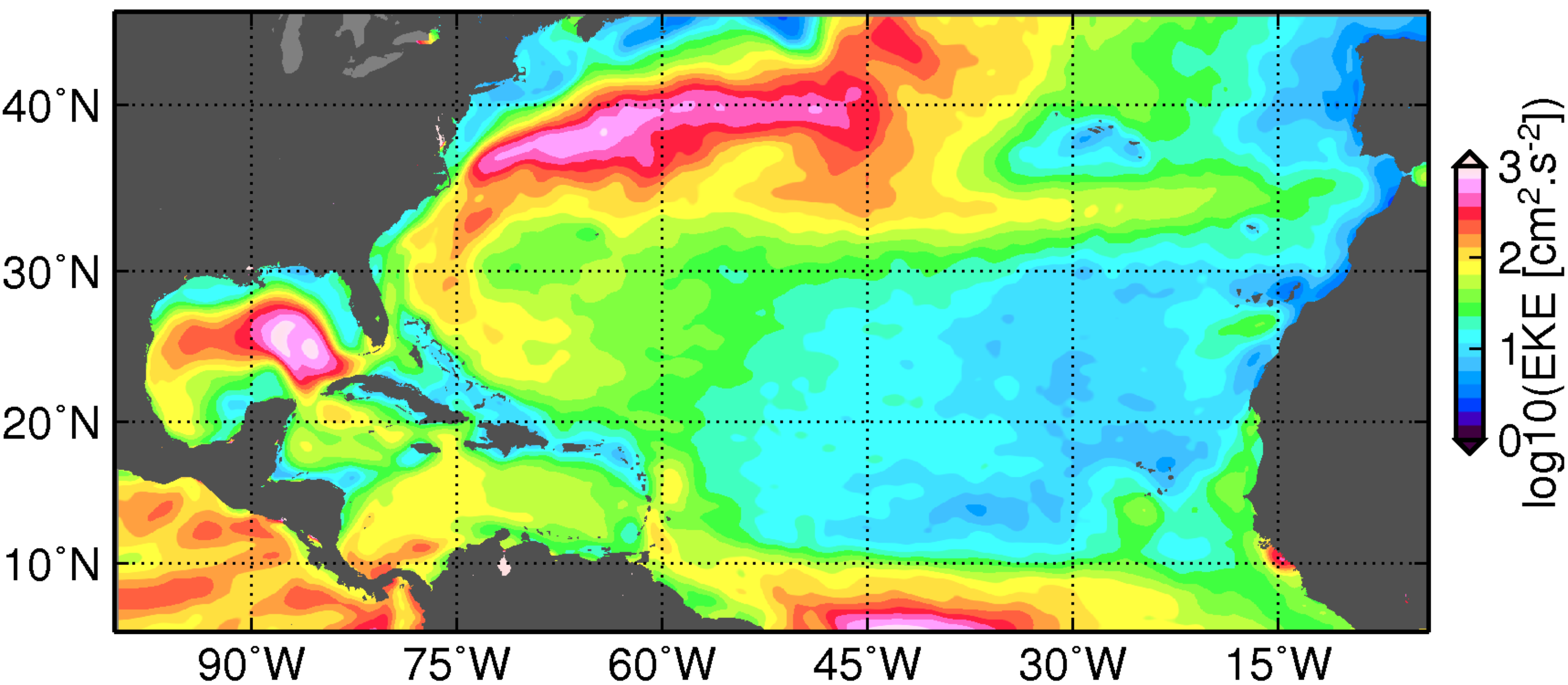

40°N
30°N
20°N
10°N
90°W
75°W
60°W
45°W
30°W
15°W
3
2
1
0
log10(EKE [cm^2.s^{-2}])

Figure 3. Figure

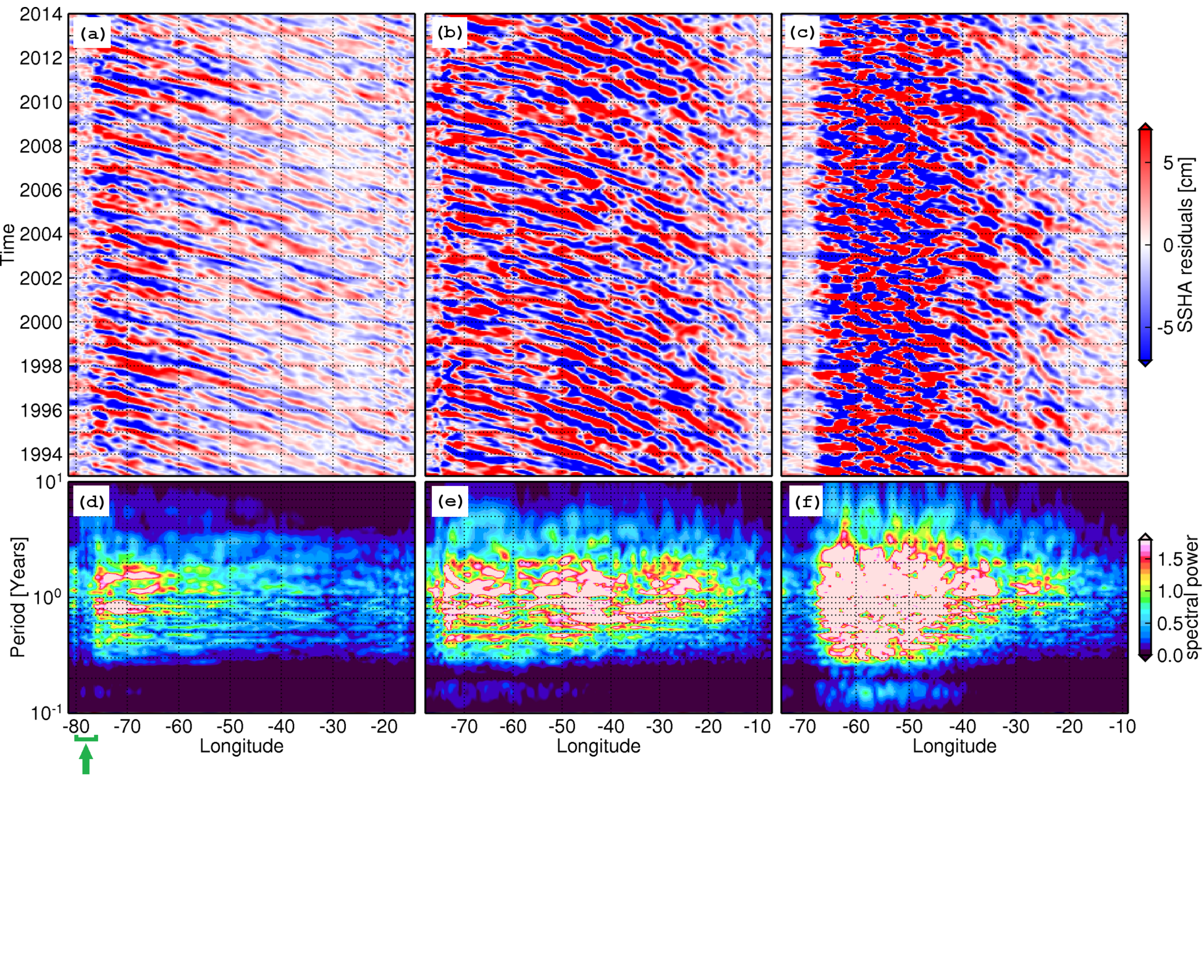

(a)
(b)
(c)
(d)
(e)
(f)
Time
Period [Years]
Longitude
SSHA residuals [cm]
spectral power

Figure 4. Figure

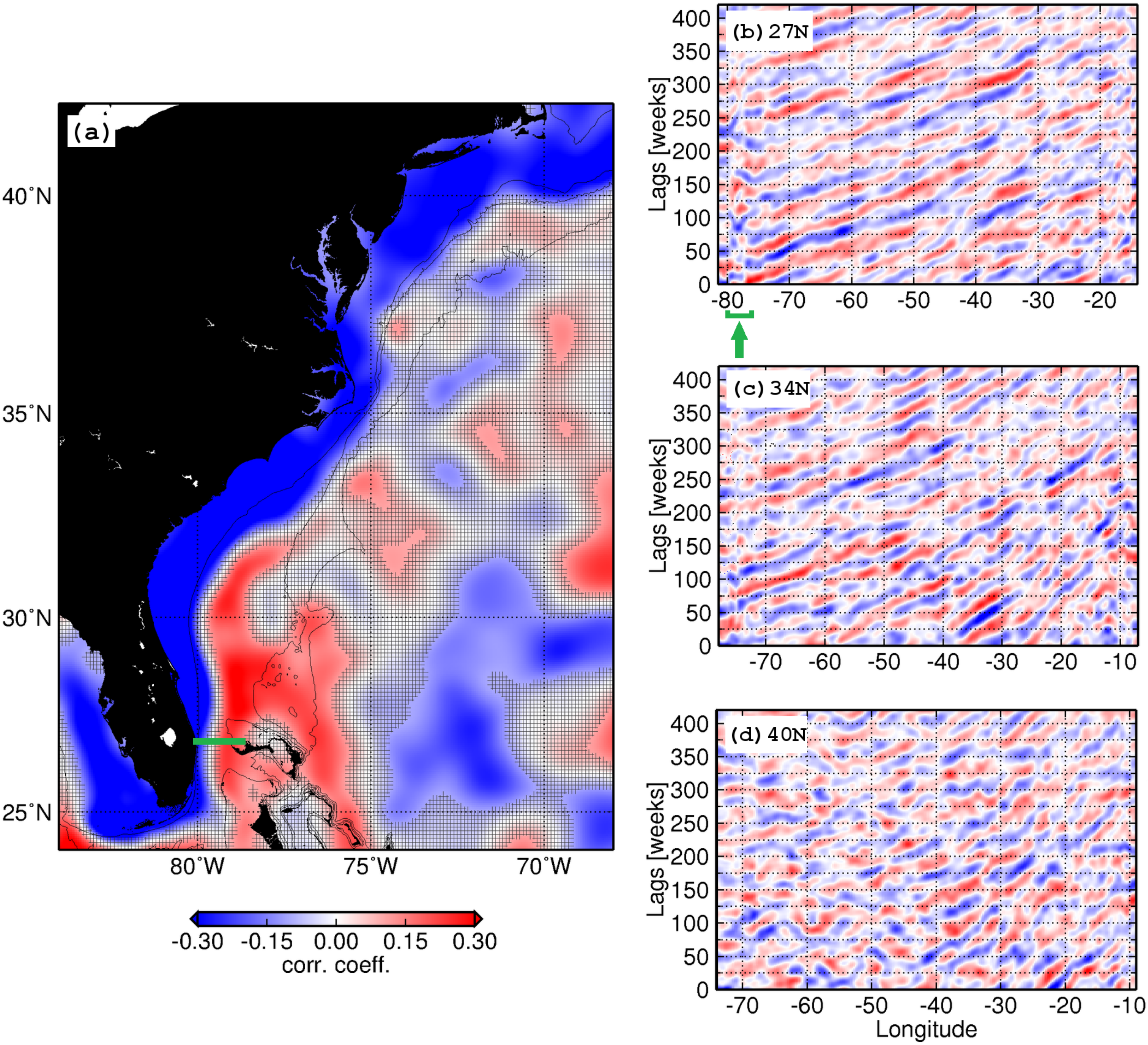

(a)
40°N
35°N
30°N
25°N
80°W
75°W
70°W
-0.30
-0.15
0.00
0.15
0.30
corr. coeff.
(b) 27N
(c) 34N
(d) 40N
Lags [weeks]
Longitude

Figure 5. Figure

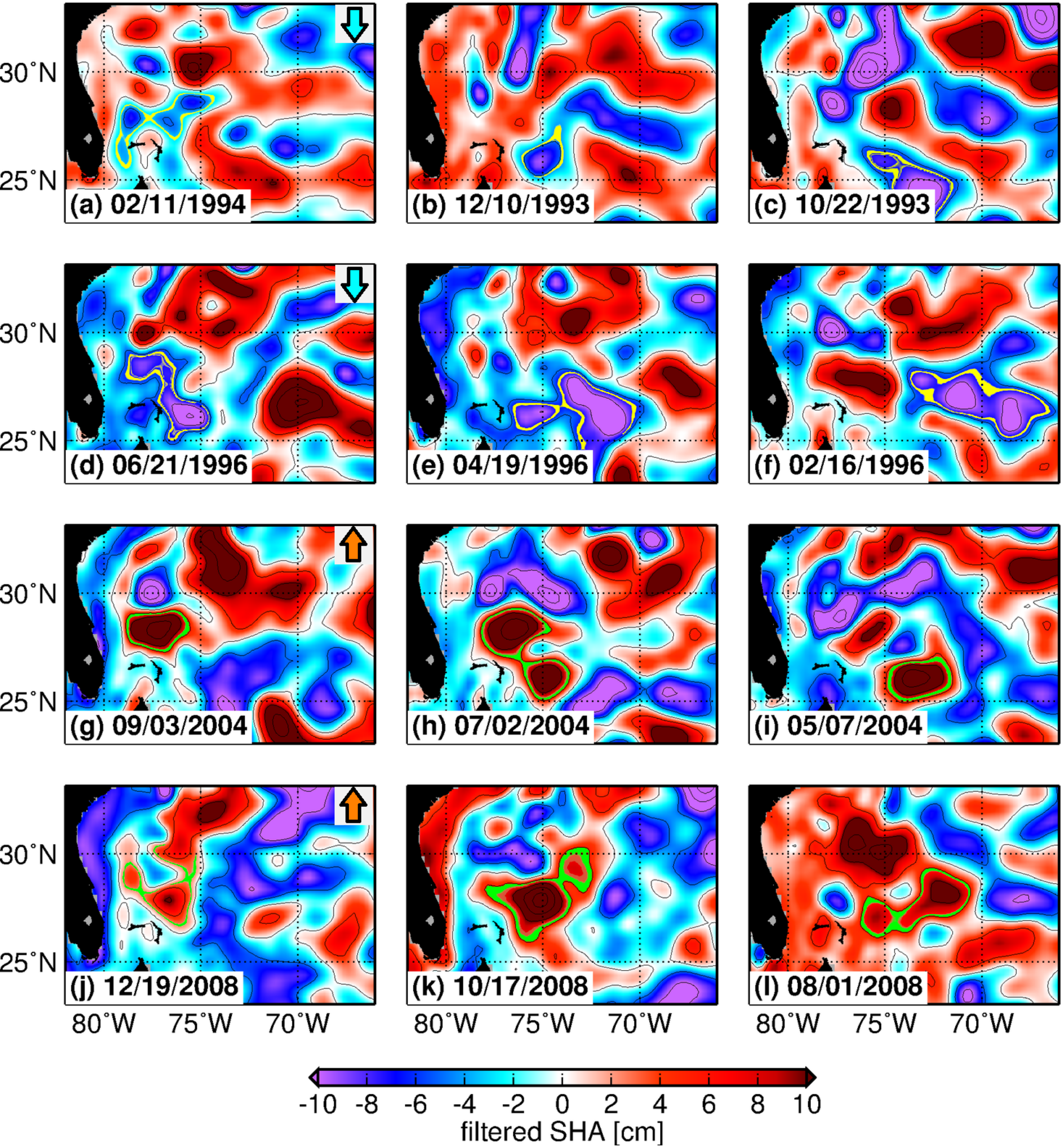

30°N
25°N
(a) 02/11/1994
(b) 12/10/1993
(c) 10/22/1993
(d) 06/21/1996
(e) 04/19/1996
(f) 02/16/1996
(g) 09/03/2004
(h) 07/02/2004
(i) 05/07/2004
(j) 12/19/2008
(k) 10/17/2008
(l) 08/01/2008
80°W
75°W
70°W
-10
-8
-6
-4
-2
0
2
4
6
8
10
filtered SHA [cm]

Figure 6. Figure

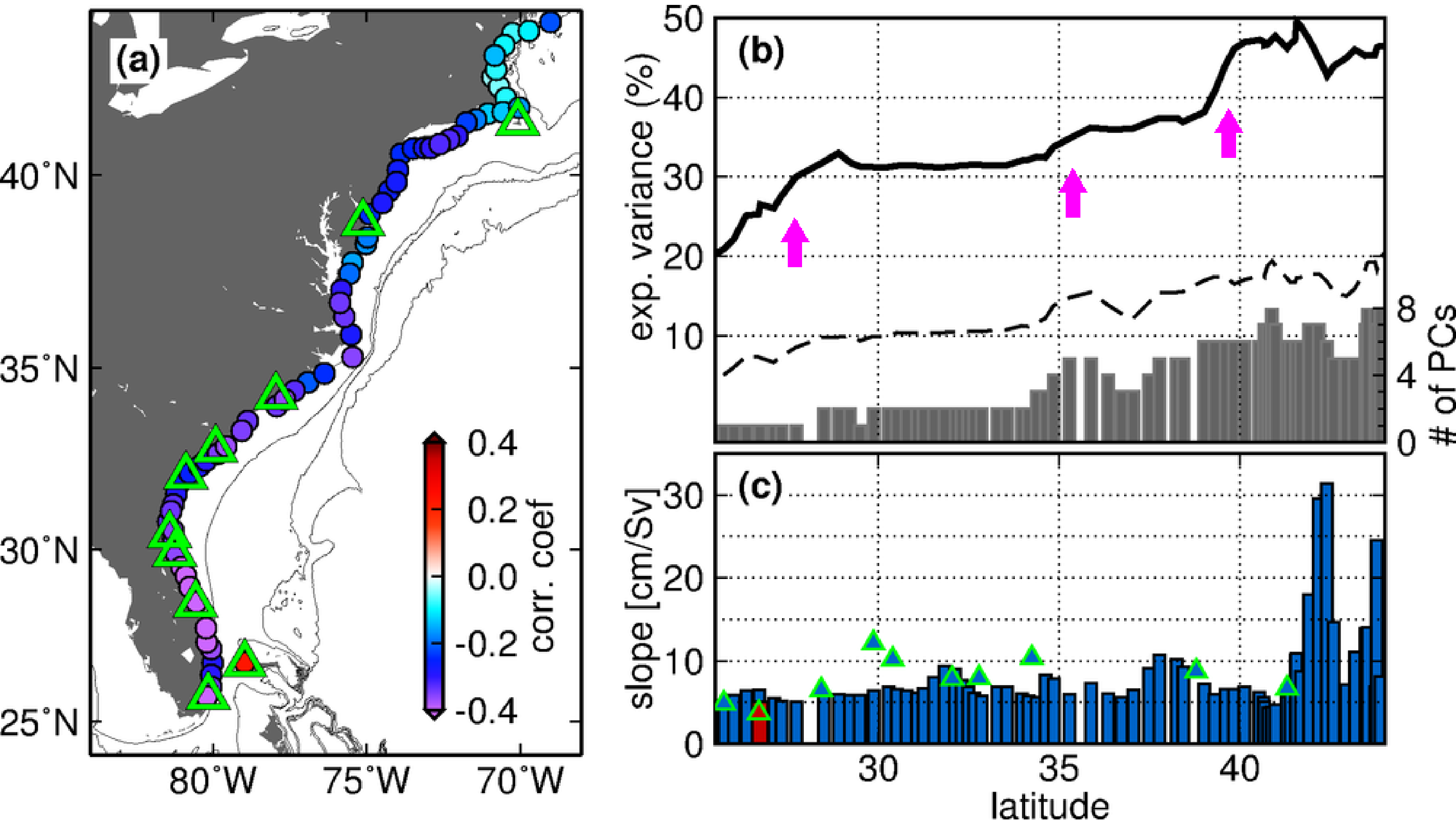

(a)
40°N
35°N
30°N
25°N
80°W
75°W
70°W
0.4
0.2
0.0
-0.2
-0.4
corr. coef
(b)
exp. variance (%)
50
40
30
20
10
8
4
0
# of PCs
(c)
slope [cm/Sv]
30
20
10
0
30
35
40
latitude

Figure 7. Figure

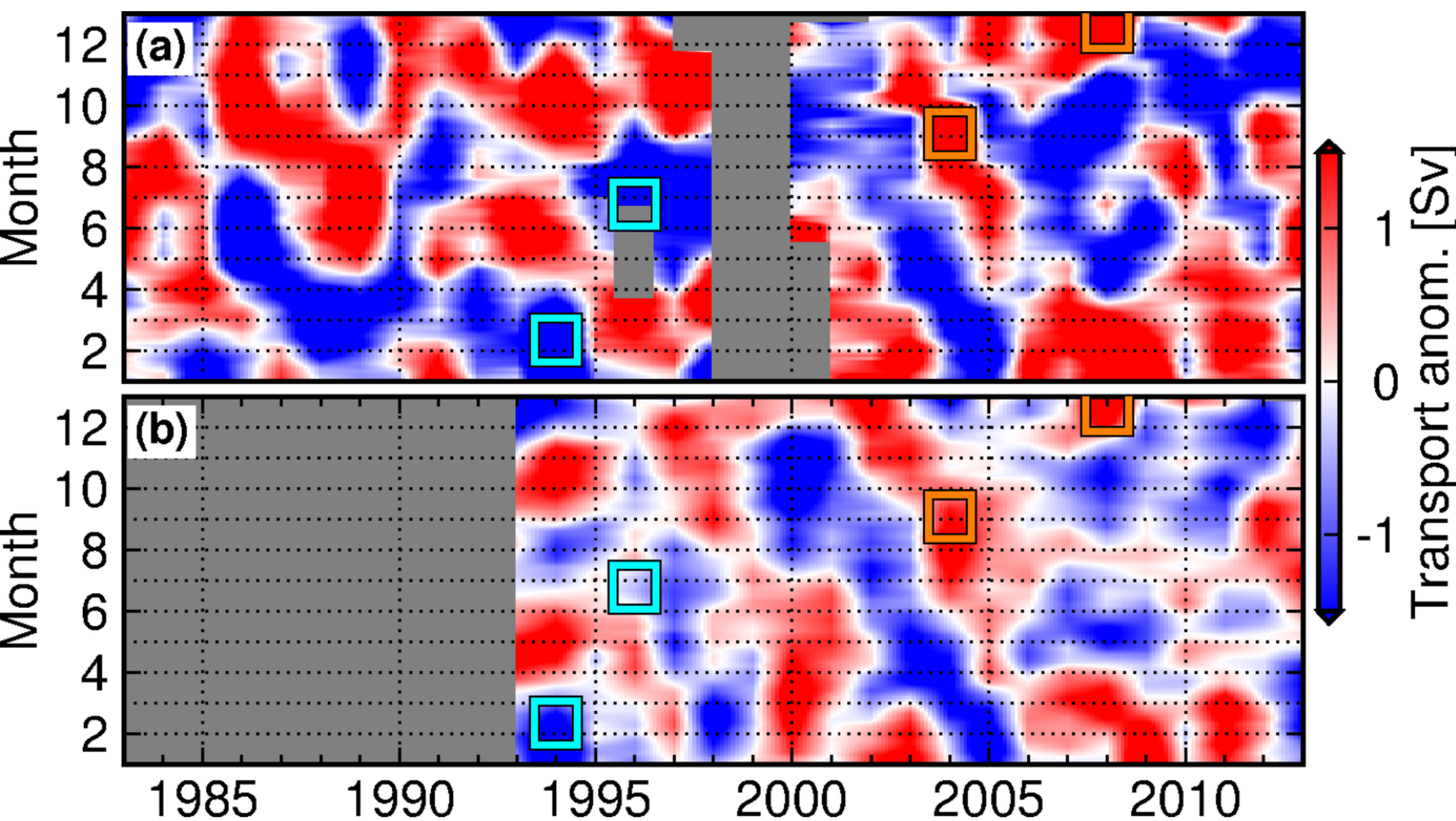

(a)
(b)
Month
Month
12
10
8
6
4
2
1985
1990
1995
2000
2005
2010
Transport anom. [Sv]
1
0
-1